Chapter 2
Subsidence Due to Hydrocarbon Production in the Netherlands

In this chapter, the mechanism of subsidence due to hydrocarbon production is described. Subsidence at ground level is caused by the compaction of the reservoir rock due to hydrocarbon extraction. The spatial and temporal development of subsidence is dependent on the production rate, the physical reservoir rock properties and the overlying subsurface layers. In the Netherlands, subsidence monitoring is legally obliged to control the water management and to avoid environmental damage. Moreover, it provides information on reservoir behavior and well performance, for example to control steam injection for the optimization of oil production.

Section 2.1 starts with a brief overview of the geological circumstances that are required for the existence of hydrocarbon reservoirs. Subsequently, the geophysical properties of gas and oil reservoirs in the Netherlands, in particular the Groningen gas field, are discussed in more detail. Based on the reservoir parameters, models that have been developed for subsidence prediction are described. The actual subsidence measurements in the Netherlands are described in Sect. 2.2. Section 2.3 gives an overview of the subsidence estimation methodologies that have been applied since the start of gas extraction from the Groningen field.

2.1 Geological Background

In this section, the existence and properties of hydrocarbon reservoirs are discussed, followed by an explanation of the Groningen gas reservoir.

2.1.1 Hydrocarbon Reservoirs

Hydrocarbon is formed from organic debris exposed to high temperature and pressure due to increasing overburden (overlying sediments) in time (Chapman, 1983; Landes, 1959; Rondeel et al., 1996). It is stored in reservoir rock, where void spaces can be filled with water, hydrocarbon liquids (oil) or hydrocarbon gas. The most common reservoir rocks are sandstones and carbonates. The hydrocarbon compo-

V.B.H. (Gini) Ketelaar, *Satellite Radar Interferometry,*
Remote Sensing and Digital Image Processing 14,

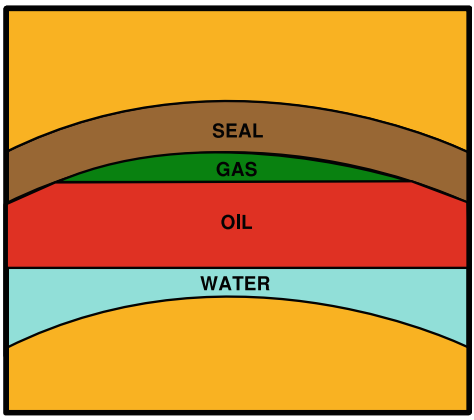

Fig. 2.1 Hydrocarbon accumulation in an anticlinal trap. The seal prevents the hydrocarbon fluids from migrating further upwards. Water, oil and gas are layered according to their density

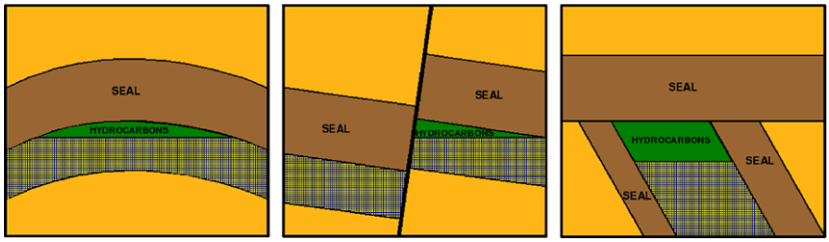

Fig. 2.2 Structural traps: anticlinal trap (left) and fault trap (middle). Stratigraphic trap (right): tilted layers of varying permeability

sition of a reservoir depends on the type of hydrocarbons, the temperature and the pressure in the reservoir. The fluids within a reservoir are layered according to their density, see Fig. 2.1.

Since the hydrocarbons tend to migrate upwards, a seal and a trap are required for hydrocarbons to accumulate. A seal consists of material that is impervious for hydrocarbon fluids. Examples of seals are shales or evaporites (such as salt layers). A trap is an enclosed reservoir that is that is surrounded by impervious rock. Traps are subdivided into structural and stratigraphic traps, see Fig. 2.2. Examples of structural traps are anticlines, faults and salt core structures. Stratigraphic traps are caused by changes in permeability. Tilting of sedimentary layers is often required for such a trap to exist (ibid.).

For a profitable extraction of hydrocarbons, a reservoir must meet certain quality criteria. Besides the hydrocarbon volume, the thickness and extent of the reservoir, porosity and permeability are driving factors. Porosity is the percentage of the total reservoir rock volume that is void space. Although porosity is required for hydrocarbon storage, it does not guarantee that the hydrocarbon fluids are able to flow in the reservoir. The ability of a rock to transmit fluid and discharge its hydrocarbon contents is defined as the permeability. The higher the permeability of a reservoir rock, the easier the hydrocarbon fluids will flow. Porosity and permeability are dependent

on grain shape, packing and sorting, degree of cementation and the overburden. For more information, see Craft and Hawkins (1991) and Dake (2002).

2.1.2 The Groningen Reservoir

The subsurface of the Netherlands contains numerous gas fields and several oil reservoirs. The majority of the hydrocarbon reservoirs is situated in the northeastern part of the Netherlands, see Fig. 2.3. Oil and gas production in the Netherlands has started with the discovery of the Schoonebeek oil field in 1943 and the Coevorden gas field in 1948. The Groningen gas field was discovered in 1959.

The geology of the Groningen gas field is depicted in Fig. 2.4. The gas has been formed in the Carboniferous period (365–290 million years ago). Subsequently, it has migrated upwards to the porous sandstones in the Rotliegend layer from the Permian period (290–250 million years ago). These sandstone layers have been formed from aeolian and fluvial deposits (de Jager and Geluk, 2007). The aeolian deposits form the best reservoirs since the grains are well sorted. The gas reservoirs are sealed by the Ten Boer claystone layer and the thick Zechstein salt layer. The boundaries of the Groningen gas reservoir are mainly defined by fault zones, with a few closures that are caused by the orientation of the layers with respect to the horizontal plane (NAM, 2003c).

The Groningen gas field has a horizontal extent of approximately 900 km^2. It is situated at a depth of 2750–2900 m and its thickness varies between 100 and 200 m (NAM, 2005). Porosity values vary between 16 and 20% (Teeuw, 1973). The Groningen gas field is the largest gas field in western Europe and one of the largest gas fields in the world. The estimated recoverable volume is $\sim$2700 billion m^3. The total number of wells that has been established is 295, arranged in 29 clusters. Gas production has started in 1963. Currently, the focus lies primarily on the gas production from the smaller gas fields in the Netherlands (NAM, 2003c). The production from the Groningen gas field is kept relatively low ($\sim$30 billion m^3 per year) to increase its lifetime.

Since the focus of this book lies on subsidence monitoring, the reader is referred to Duin et al. (2006); Lutgert et al. (2005), and Breunese et al. (2005) for a detailed description of the geology of the Netherlands and the performance of gas production from the Groningen field.

2.1.3 Reservoir Properties

This section explains the reservoir properties that determine the potential amount of subsidence due to hydrocarbon production. First, the driving factors for the compaction of the reservoir are explained. Secondly, the influence of faults and aquifers are explained.

Fig. 2.3 Overview of the location and spatial extent of the Groningen gas field, including the well locations and the faults (NAM, 2003c)

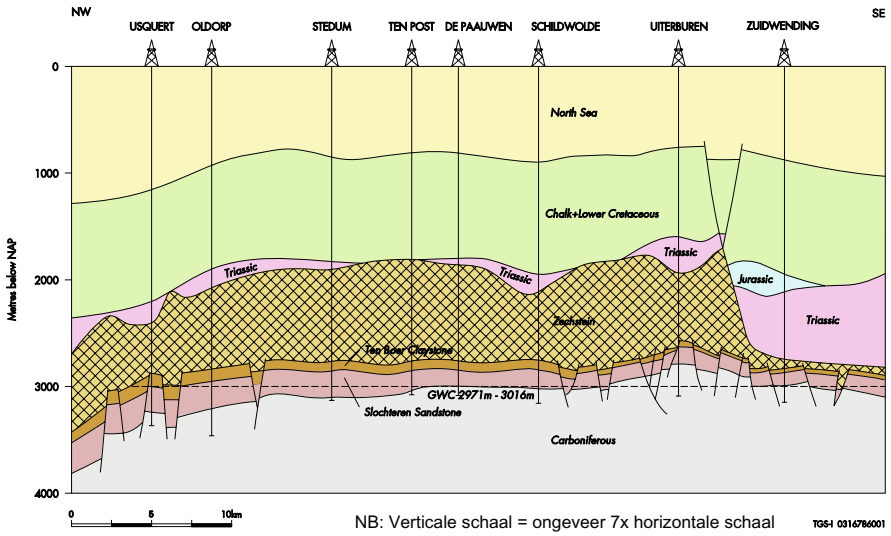

Fig. 2.4 Cross-section of the Groningen gas field (NAM, 2003c). The location of this cross-section is indicated in Fig. 2.3 as 'Line of Section'. The Slochteren sandstone formation is part of the Rotliegend layer

2.1.3.1 Reservoir Compaction

During the production of gas and oil, the pore pressure decreases. Because the overburden remains unchanged, the effective stress on the grain structure of the reservoir increases. As a result, the reservoir is compacting: its volume decreases. If the lateral dimension of the reservoir is large compared to its thickness, compaction mainly results in a reduction of reservoir height (Geertsma, 1973b). Hence, reservoir compaction can initially be characterized by the vertical strain ε_z in the reservoir:

$$\varepsilon_z = \frac{dz}{z}, \tag{2.1}$$

which is the change in reservoir height dz relative to its initial height z, caused by an increase in effective stress due to a decrease in pore pressure dp under a constant overburden. Reservoir compaction in vertical direction is characterized by the uniaxial compaction coefficient c_m:

$$c_m = \frac{1}{z}\frac{dz}{dp}, \tag{2.2}$$

that describes the compaction per unit change in pore pressure (in bar^{-1}). The total compaction ΔH until a certain point in time is dependent on the difference in pore pressure Δp since the start of the production and the initial reservoir thickness H:

$$\Delta H = c_m \cdot \Delta p \cdot H. \tag{2.3}$$

The compressibility of the reservoir rock in lateral direction is specified by Poisson's ratio ν. Poisson's ratio is the ratio between the lateral strain and the vertical strain. Its value is ~0.25 for the Groningen gas field. Section 2.1.4 shows that subsidence at surface level depends both on the uni-axial compaction coefficient and Poisson's ratio.

2.1.3.2 The Compaction Coefficient

The compaction coefficient is dependent on the physical reservoir properties. There are two methods available to derive the compaction coefficient: by laboratory tests on core samples from the wells (Teeuw, 1973), and by means of radio-active bullets that have been shot in the reservoir at observation wells (de Loos, 1973; NAM, 2005).

Core samples have been taken from wells in different parts of the Groningen gas field. In the laboratory, the behavior of the reservoir rock under in situ stress conditions has been analyzed. The reservoir compaction is determined from the relative change in reservoir thickness due an increase in effective vertical stress under zero lateral strain.

Besides by performing laboratory tests on core samples, compaction can be measured in situ. The measurement targets for in situ compaction measurements are radio-active bullets that have been shot in the formation at regular distance. Their relative displacement is measured periodically by means of a gamma-ray detector. This gamma-ray detector is connected to a cable that is deployed in an observation well. In the Groningen gas field, eleven observation wells have been established where these in situ compaction measurements are carried out with millimeter precision (NAM, 2005). The compaction measurements show a linear dependency on the reservoir pressure. The compaction coefficient c_m that has been deduced from these measurements varies between 0.45 and $0.75 \cdot 10^{-5}$/bar (ibid.).

The initial pressure in the Groningen reservoir was 347 bar, which has dropped to 125 bar in 2005 (ibid.); the average thickness of the reservoir is 170 m. Using (2.3), this would imply that gas production up to 2005 has caused a total reservoir compaction between 17 and 28 cm. The resulting compaction at ground level is dependent on the depth and radius of the reservoir and Poisson's ratio as well, see Sect. 2.1.4. Furthermore, reservoir compaction may be subject to a delay in time (Hettema et al., 2002), in which the reservoir reconverges to an equilibrium and the compaction propagates through the overburden to ground level.

The amount of reservoir compaction is also driven by the reservoir rock properties: ordering, shape and hardness of the grains, and the degree of cementation or frame rigidity (Teeuw, 1973). The rock properties also determine whether the deformation is reversible or not. The deformation of hard rock exhibits in general elastic (reversible) behavior. The compaction of soft rock may be partly irreversible due to crushing and relocation of grains. Rock types are subdivided in tight rock, well-consolidated rock, semi-consolidated rock and unconsolidated rock, with varying porosity from 0 to 40%, and an increasing compaction coefficient. The Groningen Rotliegend reservoir is classified as semi-consolidated, and elastic behavior is assumed.

2.1.3.3 Reservoir Connectivity

The amount of reservoir compaction is dependent on the thickness of the reservoir, the pressure drop in the reservoir, and the compaction coefficient of the reservoir rock. If these parameters vary through a reservoir, the reservoir compaction will vary as well. Discontinuous changes can be found near faults. Depending on the reservoir thickness, the vertical offset, the orientation of the faults, and the depth of the gas-water contact, they can be sealing or not. If the drainage region of a well contains sealing faults, the well will not produce hydrocarbons from the disconnected block. As a result, there will a be compacting and non-compacting block on either side of the fault. The fault pattern of the Groningen gas field is depicted in Fig. 2.3. It has a dominantly southeast–northwest orientation. The interaction between the reservoir blocks can impose an uncertainty on the subsidence prediction.

2.1.3.4 Aquifers

In Sect. 2.1.1 it has been explained that a reservoir can be partly filled with water. The part of the reservoir that is filled with water is called the aquifer. Due to the higher density of the water, the aquifer will be located below the hydrocarbon fluids. The presence and dimensions of the aquifer determines the pressure drop during hydrocarbon production. If the aquifer is large with respect to the gas reservoir, it can provide pressure support to the hydrocarbon reservoir (NAM, 2005). If the aquifer is small, hydrocarbon production can significantly affect the aquifer pressure. Since the aquifer partly determines the pressure distribution within the reservoir, knowledge on the depletion of aquifers is important for the estimation of reservoir compaction. Moreover, uncertainties can exist about the connection of lateral aquifers around fault zones. Since there are hardly any wells established in the aquifer zones, there is a lack of observations on their pressure behavior. Geodetic measurements at ground level, such as leveling and PSI, can provide knowledge on the depletion of aquifers. For example, based on the leveling campaigns, it could be concluded that the aquifer to the west of the Groningen gas field is not depleting (ibid.).

2.1.4 Subsidence Prediction Methodologies

Based on the geophysical properties of the hydrocarbon reservoir and the overlying layers, subsidence at ground level can be predicted. Various methods have been applied: analytical (Geertsma, 1973a), semi-analytical (Fokker, 2002; Fokker and Orlic, 2006), numerical (Sroka and Hejmanowski, 2006) and finite element methods (Geertsma and van Opstal, 1973; Fredrich et al., 2000).

The analytical solutions for subsidence prediction that are described by Geertsma (1973a) assume that the overburden is uniform and elastic. The reservoir itself is

built up of so-called 'nuclei-of-strain' that have a small but finite volume V. The vertical displacement u_z caused by a nucleus-of-strain is given by:

$$u_z(r,0) = -\frac{c_m(1-\nu)}{\pi}\frac{D}{(r^2+D^2)^{3/2}}\Delta pV, \tag{2.4}$$

where:

r	radial distance from the vertical axis through the nucleus-of-strain,
c_m	uni-axial compaction coefficient$(\text{kg/cm}^2)^{-1}$, see (2.2),
ν	Poisson's ratio,
Δp	pore pressure reduction (kg/cm^2),
D	depth of burial of the nucleus-of-strain,
V	volume of the nucleus-of-strain.

A negative vertical displacement implies subsidence, whereas a positive vertical displacement implies uplift. The geometrical shape of the displacement induced by a nucleus-of-strain is equal to the displacement induced by a point source as defined by Anderson (1936) and Mogi (1958).

Surface deformation due to hydrocarbon production is not restricted to vertical displacements. The horizontal displacement u_r due to a nucleus-of-strain reads:

$$u_r(r,0) = +\frac{c_m(1-\nu)}{\pi}\frac{r}{(r^2+D^2)^{3/2}}\Delta pV, \tag{2.5}$$

where a positive horizontal displacement is in the direction towards the location of the nucleus-of-strain. From (2.4) and (2.5) it is deduced that the ratio between horizontal and vertical displacements equals $-r/D$.

The total subsidence above a reservoir can subsequently be obtained by the integration of the nucleus-of-strain solutions over the entire reservoir. A closed form solution of the integration of the nucleus-of-strain solutions is given by Geertsma (1973a), based on a simplified representation of the reservoir as a disc-shaped reservoir of thickness H and radius R at depth D. The pressure reduction Δp is assumed to be uniform through the reservoir. The equations are non-linear and require the evaluation of Hankel-Lipschitz integrals. The maximum vertical displacement above a disc-shaped reservoir can be expressed analytically:

$$u_z(0,0) = -2c_m(1-\nu)\Delta pH\left(1-\frac{D/R}{\sqrt{1+(D/R)^2}}\right). \tag{2.6}$$

Apart from the compaction coefficient, Poisson's ratio, the pressure drop and the thickness of the reservoir, the ratio between the depth and the radius of the reservoir determines the maximum amount of subsidence.

The analytical expressions for subsidence prediction are based on a simplified representation of the subsurface. The reservoir is not a perfect disc; nor is the overburden perfectly homogeneous. Hejmanowski and Sroka (2000) subdivide the reservoir into elementary cubicoids with each their own geomechanical properties (thickness, compaction, pressure drop). Subsequently, influence functions are applied to

estimate subsidence due to a reservoir element at surface level. The total subsidence is the superposition of the contributions of all reservoir elements. Finite element methods utilize a geomechanical model of the entire subsurface: the reservoir and the adjacent geological layers, up to ground level. Fredrich et al. (2000) model the evolution of the displacements in the Belridge reservoir and the overburden, based on such a finite element model.

Finite element models have the advantage that they can be applied to reservoirs of arbitrary geometry with varying reservoir properties and pressure distribution, see e.g., Geertsma and van Opstal (1973). Hence, a more accurate prediction of vertical displacements and horizontal gradients can be obtained, provided that the distribution of deformation properties in the reservoir is known sufficiently. Moreover, the overburden can be modeled more accurately in finite element models. A disadvantage of finite element methods is the computation time. Hence, semi-analytical modeling (Fokker, 2002; Fokker and Orlic, 2006) has been introduced. Semi-analytical modeling avoids the time consuming finite element approach, but uses a more sophisticated model for the subsurface compared to the analytical solutions of Geertsma (1973a). Instead of assuming a homogeneous subsurface, the subsurface is divided into multiple layers with each their own (visco-)elastic properties.

Both the analytical method from Geertsma (1973a) (with the reservoir subdivided into smaller blocks) and finite element analysis have been applied to predict subsidence due to hydrocarbon production in the Netherlands (NAM, 2005). Since the results of both methods are comparable, the analytical method is used for the majority of the gas fields (ibid.). Finite element analysis has been applied to calculate subsidence above the Ameland reservoir: it is located below a complicated salt structure which behavior cannot be modeled using the analytical method (ibid.).

2.2 Subsidence Monitoring Using Leveling Measurements

This section addresses the leveling campaigns that have been performed for subsidence monitoring in the Netherlands, and the legal guidelines.

2.2.1 Leveling Campaigns

Since the start of gas production in Groningen in the 1960s, leveling campaigns have been performed periodically. Leveling is an optical land surveying technique that measures height differences between established benchmarks. These benchmarks are spatially distributed over the area of interest and are ideally a discretization of the shape of the subsidence pattern. By measuring the benchmark height differences in multiple epochs, the development of the subsidence bowl(s) is monitored.

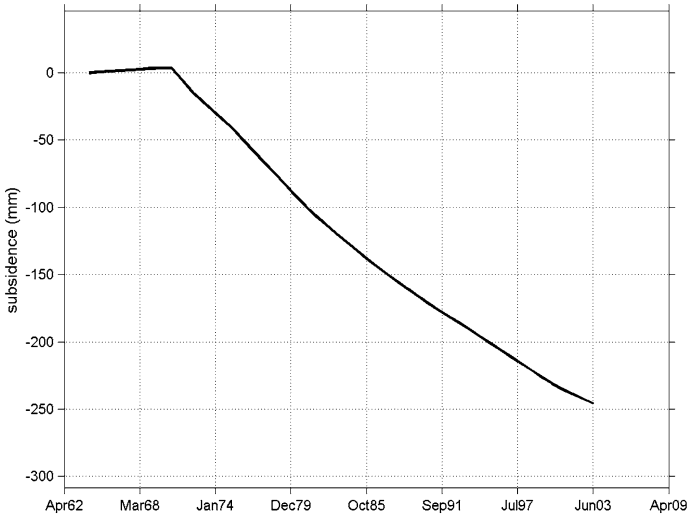

Fig. 2.5 Subsidence (mm) since the start of gas production in the center of the Groningen subsidence bowl, estimated from leveling observations (Schoustra, 2004). The subsidence rate has slightly decreased after the change of priority to the smaller gas fields from the 1970s

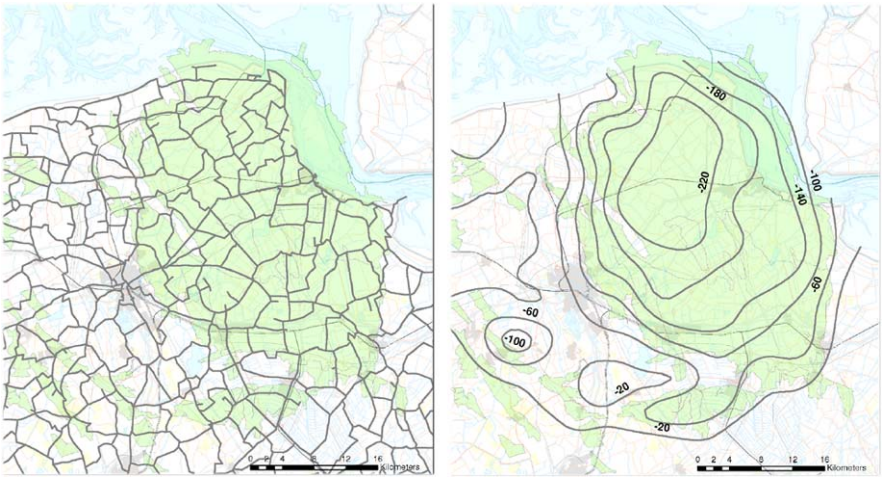

Fig. 2.6 Leveling network of the 2003 campaign (left) and subsidence (mm) since the start of gas production up to 2003 (right). The gas fields are depicted in green. The total length of the leveling trajectories is ∼1000 km. Source topographic background: © Kadaster en de Openbare Registers, Apeldoorn

Since subsidence measurements are decisive for taking environmental countermeasures, the quality assessment of the estimated height differences is crucial. Redundant measurements have been taken in order to test observations on measurement errors and systematic errors. Figure 2.6 shows the leveling loops in the north-

eastern part of the Netherlands. Subsidence due to gas extraction has been estimated from repeated leveling campaigns since the start of the production. The deepest point in the Groningen subsidence bowl has subsided 24.5 cm until 2003 (Schoustra, 2004), see Fig. 2.5. In time, the displacements are approximately linear. After the 1970s the displacement rate has slightly decreased, after the priority has been shifted to the smaller gas fields. The Groningen gas field and the underground gas storages in Norg and Grijpskerk have the role of swing producer, covering peaks in demand (NAM, 2008).

Benchmark heights are orthometric and refer to the local Dutch height reference system 'Normaal Amsterdams Peil' (NAP). Since leveling is a relative technique, all heights are estimated with respect to a reference benchmark.

2.2.2 Legal Guidelines

Monitoring surface deformation due to mineral extraction is legally obliged in the Netherlands according to the Dutch mining legislation (Mijnbouwwet, 2008). Oil, gas and salt mining companies are obliged to develop and update measurement plans that need to be approved by the Ministry of Economic Affairs. According to the mining legislation, these measurement plans should contain the points in time, the location of the measurements, and the measurement techniques. One measurement campaign needs to be performed prior to the start of the production. The State Supervision of Mines (the mining authority) supervises all mining activities in the Netherlands, including the estimation of subsidence due to mineral extraction. Its mission is to ensure that the exploration and production of minerals in the Netherlands and the Dutch part of the continental shelf is carried out in a responsible and socially acceptable manner (SodM, 2008).

Duquesnoy (2002) defines further guidelines for subsidence monitoring using the leveling technique. A condition that is imposed on the leveling measurements is their agreement with the precision criteria as defined by AGI (2005). Examples of these precision criteria are the critical values for the misclosures of leveling loops and the precision of the height difference observations.

Furthermore, Duquesnoy (2002) investigates the spatial and temporal observation density. The required spatial benchmark density is dependent on the shape and extent of the subsidence bowl. Guidelines are provided based on a simplified representation of the gas reservoir. The Groningen gas field may be approximated by a disc-shaped reservoir of radius 15 km at a depth of 3 km. Based on an angle of draw of 45 degrees, the subsidence border is located at 18 km from the center of the reservoir. Application of the guidelines of Duquesnoy (2002) would imply a benchmark density of 1 per km^2 in the deepest part of the bowl and outside the subsidence border. At the slopes, a slightly higher spatial density (1.5 benchmark per km^2) is required to reconstruct the spatial subsidence pattern.

The determination of the measurement frequency is dependent on the precision of subsidence measurements. A new measurement campaign will only contribute if the

expected subsidence is significant compared to the measurement precision. Moreover, the subsidence history based on preceding measurements can be utilized to predict subsidence with a higher precision. In this way, the measurement frequency can be lowered as the monitoring period increases, provided that the production rate does not change significantly and the compaction process is linear elastic. However, for practical reasons, a maximum period of 5 years is maintained between two measurement campaigns (ibid.).

2.3 Geodetic Deformation Monitoring

Geodetic techniques for deformation monitoring have been refined through the years. From the estimation of benchmark height differences, deformation monitoring has been extended with the parameterization of the temporal and spatial behavior of the deformation phenomenon. Moreover, dynamic systems that describe the forces and loads that cause the deformation and the physical properties of the deformation mechanism can be included, see e.g., Welsch and Heunecke (2001). Hence, advanced deformation analysis requires an interdisciplinary approach that integrates geodetic and geophysical skills.

This section provides an overview of deformation monitoring methodologies that have been applied to estimate subsidence due to gas extraction in the Netherlands. It starts with an overview of geodetic adjustment and testing techniques. Subsequently, point-wise multi-epoch deformation analysis is explained. This type of analysis is followed by the estimation of continuous spatio-temporal deformation phenomena.

2.3.1 Adjustment and Testing Procedure

The adjustment and testing procedure underlying geodetic deformation monitoring performs the estimation of unknown parameters and testing on observational and model errors in an integrated way. The testing procedure is important in deformation analysis, since the optimal parameterization of the unknowns is often less well known compared to classical geodetic applications, such as cadastral surveys. For example: the spatial shape of subsidence due to gas extraction has a higher degree of uncertainty than the location of the corner of a house. Hence, multiple alternative hypotheses are evaluated to determine the mathematical model that minimizes the least-squares residuals with respect to the observations. In this way, the optimal deformation model is found for the signal of interest. Of course each of the models under the alternative hypotheses should be physically explainable, to avoid fitting a non-realistic model to the observations. This section summarizes the mathematical framework of the adjustment and testing procedure.

The system of equations under the null hypothesis H_0 is formulated as a Gauss-Markov model:

$$H_0: \qquad E\{\underline{y}\} = Ax; \qquad D\{\underline{y}\} = Q_y, \tag{2.7}$$

where $\underline{y}$ is the vector of observations, x are the unknown parameters, and the design matrix A specifies the functional relation between them. The underlining of a vector (such as $\underline{y}$) indicates its stochastic character; the variance-covariance matrix of the observations is represented by Q_y.

Estimates of the unknown parameters are obtained by least-squares adjustment (Teunissen, 2000a). Subsequently, the validity of the null hypothesis is tested in the Detection, Identification and Adaptation (DIA) procedure (Teunissen, 2000b). In the **Detection** step, the null hypothesis is tested by means of the overall model test (OMT):

$$\underline{T}_{q=m-n} = \underline{\hat{e}}^T Q_y^{-1} \underline{\hat{e}}; \qquad \text{reject } H_0 \text{ if } T_{q=m-n} > \chi^2_\alpha(m-n, 0), \tag{2.8}$$

which is dependent on the least-squares residuals $\underline{\hat{e}}$ and the variance-covariance matrix of the observations. The redundancy $m-n$ equals the number of observations minus the number of unknowns (provided that the design matrix is of full rank).

If the overall model test is rejected, alternative hypotheses can be specified that are evaluated in the **Identification** step:

$$H_a: \qquad E\{\underline{y}\} = Ax + c_y \nabla, \tag{2.9}$$

where ∇ represents the model error and c_y specifies the functional relation with the observations that can be multi-dimensional. A standard test is datasnooping, where individual observations are checked for blunders. In this case, c_y will have the shape

$$c_{y_i} = (0, \ldots, 0, 1, 0, \ldots, 0)^T \tag{2.10}$$

for the ith observation.

The functional model that parameterizes the signal of interest is often not very well known a-priori in deformation monitoring. Therefore, multiple tests of different dimensions are specified to trace different kinds of model deviations. In the evaluation of tests of different dimensions, the one with the lowest teststatistic does not necessarily correspond with the most likely alternative hypothesis. This is caused by the different probability density functions for tests of different dimensions. A solution is provided by de Heus et al. (1994) by introducing testquotients: the ratio of teststatistics and their critical values. Provided that the power of the test is set to 50%, testquotients can be directly compared.

The **Adaptation** step involves either remeasuring and replacing (a part of) the observations or the replacement of the null hypothesis by the most likely alternative hypothesis. To test the validity of the mathematical model after adaptation, the DIA procedure is performed in an iterative way.

Besides the functional model, the stochastic model can be re-evaluated as well by means of variance component estimation (VCE) (Teunissen, 1988; Amiri-Simkooei, 2007). The stochastic model is then decomposed for the estimation of the variance factors σ_k^2:

$$Q_y = \sum_{k=1}^{p} \sigma_k^2 Q_k, \tag{2.11}$$

where Q_k are the cofactor matrices. The estimates for the variance components $\underline{\hat{\sigma}}$ are obtained by solving the following system of equations:

$$\underline{\hat{\sigma}} = N^{-1} l, \tag{2.12}$$

where:

$$N_{kl} = \mathrm{tr}(Q_y^{-1} P_A^{\perp} Q_k P_A^{\perp} Q_l); \qquad l_k = \underline{\hat{e}}^T Q_y^{-1} Q_k Q_y^{-1} \underline{\hat{e}}, \tag{2.13}$$

where k and l are the row and column index for the kth and lth variance factor. The required input for VCE stems from the mathematical model and the adjustment results:

$\underline{\hat{\sigma}}$	the estimator for the variance components σ_k^2,
$P_A^{\perp}$	the orthogonal projector: $P_A^{\perp} = I - A(A^T Q_y^{-1} A)^{-1} A^T Q_y^{-1}$, and
$\underline{\hat{e}}$	vector of least squares residuals: $\underline{\hat{e}} = P_A^{\perp} \underline{y}$.

Since Q_y itself is involved in VCE, the variance factor estimates are obtained in an iterative way. The precision of the variance component estimates follows from the propagation law:

$$Q_{\hat{\sigma}} = N^{-1}. \tag{2.14}$$

Verhoef et al. (1996) describe the Detection-Identification-Adaptation procedure for deformation analysis incorporating VCE. Besides the estimation of variance factors (for example to estimate the measurement precision), other stochastic parameters such as the spatial correlation length of the residual signal can be obtained as well through VCE. The decomposition of Q_y in such a situation is explained in Sect. 4.3.

2.3.2 Point-wise Multi-epoch Deformation Analysis

In point-wise multi-epoch deformation analysis, the deformation signal of interest is represented by discrete measurement points that are monitored at subsequent points in time. An example is 1D deformation analysis using leveling measurements from multiple epochs (de Heus et al., 1994). It can be subdivided into the following steps:

1. epoch analysis: free network adjustment and testing of leveling height difference observations per epoch,
2. stability analysis: stability testing of underground benchmarks that are located outside the subsiding area,
3. deformation parameter estimation.

The last step restricts to the temporal analysis of benchmark height estimates, in a *static* or *kinematic* way. In static deformation analysis, subsidence per benchmark is computed by subtracting the estimated height from the initial height, whereas kinematic deformation analysis models the displacements in time: a polynomial is fit

through the height estimates, or an estimation is performed of geophysical parameters that are driving factors for the observed deformation.

Kinematic deformation analysis can be further subdivided into a *deterministic* and a *stochastic* approach. The deterministic approach attributes all residuals to measurement noise. The stochastic approach includes a residual component that can be addressed to model imperfections due to the simplification of the actual deformation pattern.

2.3.3 Continuous Spatio-temporal Deformation Analysis

Point-wise multi-epoch deformation analysis can be further developed to deformation analysis in which the continuous spatio-temporal evolution of the deformation phenomenon is modeled. Depending on the a-priori knowledge on the deformation signal of interest, this requires not only functional modeling, but also stochastic modeling of model imperfections. This section illustrates the application of continuous spatio-temporal deformation analysis for subsidence phenomena.

2.3.3.1 Subsidence—Functional Model

The spatial evolution of subsidence over multiple epochs can be described by, e.g., a point source model, or an ellipsoidal model, or prognosis grids, e.g., based on geomechanical modeling of the reservoir and the subsurface.

Depending on the complexity of the deformation mechanism, subsidence can optionally be estimated as a superposition of point source or ellipsoidal models.

The point source concept stems from volcanic applications. These point sources are often referred to as Mogi sources (Anderson, 1936; Mogi, 1958). Okada (1992) derives the displacement field in a homogeneous half-space due to point sources of

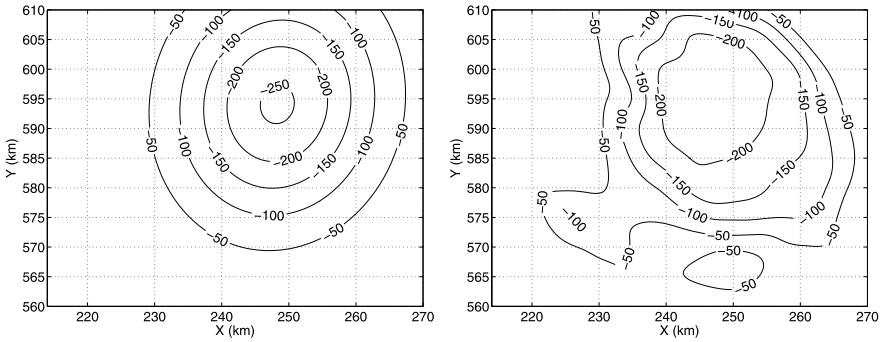

Fig. 2.7 Subsidence (mm) above the Groningen gas field estimated as a mathematical ellipsoidal shape (left) and subsidence prognosis based on geomechanical modeling of the reservoir and the subsurface (right)

different types. Specific directional point source types are defined for displacement fields due to earthquakes. If only vertical displacement due to a single point source is considered, its estimates at surface level read:

$$u_z(r,0) = M\frac{D}{(r^2+D^2)^{3/2}}, \tag{2.15}$$

where M is a multiplication factor. The physical parameters involved in this multiplication factor are dependent on the application: deformation due to gas extraction, earthquakes or volcanic activities. It can be a function of the forces acting on the deforming body, shear modulus, compaction coefficient, Poisson's ratio, pressure change, and volume changes.

Note that (2.15) is similar to (2.4). The geometrical shape of the point source model is equal to the analytical expression for the vertical displacement due to a nucleus-of-strain. The multiplication factor from (2.15) consists of the compaction coefficient, Poisson's ratio, the pressure drop and the volume of the nucleus-of-strain. The analogy of the integration over the reservoir shape (Sect. 2.1.4) would be the superposition of the contribution of multiple point sources.

The second parameterization type models subsidence as (a superposition of) ellipsoidal bowls (Kenselaar and Quadvlieg, 2001). In time, the displacement rate is assumed linear. The subsidence velocity decreases exponentially with the distance to the center of the bowl. The subsidence z at time t for point i on a certain location reads:

$$z_i^{t_0 t} = \begin{cases} \dot{z}(t-t_0)e^{-\frac{1}{2}r_i^2} & \text{for } t \geq t_0 \\ 0 & \text{for } t < t_0 \end{cases} \tag{2.16}$$

with:

$$r_i = \sqrt{\frac{((x_i-x_c)\sin\phi + (y_i-y_c)\cos\phi)^2}{a^2} + \frac{((x_i-x_c)\cos\phi - (y_i-y_c)\sin\phi)^2}{b^2}}, \tag{2.17}$$

where:

$\dot{z}$	displacement rate of point i,
r_i	distance of point i to the center of the subsidence bowl,
t_0	starting time of subsidence,
x_i, y_i	location of point i,
x_c, y_c	location of the center of the bowl,
ϕ	orientation of the bowl,
a, b	length of the ellipsoidal axes.

The last model type is the subsidence prognosis: based on geophysical reservoir behavior and the overburden, displacements are estimated in the area of interest in a regular grid that is subdivided in blocks (the grid cells). The spatial variation of geophysical parameters is taken into account in the subsidence prognosis. Hence, the subsidence prognosis is more likely to provide a realistic subsidence prediction, compared to the point source and the ellipsoidal model. The point source and the

ellipsoidal model tend to simplify the subsidence pattern. For all three model types holds that model deviations have to be assessed. If these model deviations can be explained by a geophysical mechanism, the functional model can be improved.

2.3.3.2 Subsidence—Stochastic Model

Since the functional deformation model is generally not well known a-priori, model imperfections are often incorporated in the stochastic model. This requires the model imperfections to be modeled by a covariance function that describes the spatio-temporal behavior. As a result, the variance-covariance matrix does not only contain the measurement noise component $\underline{n}$, but also the model imperfections $\underline{s}$:

$$Q_y = Q_{nn} + Q_{ss}. \tag{2.18}$$

Model imperfections comprise uncertainties in both the parameterization of the deformation signal itself and the physical representation of the measurement points. For example: if the measurement points exhibit additional autonomous movements due to shallow subsurface displacements, their displacements do not unambiguously represent subsidence due to gas and oil extraction. These autonomous movements can be stochastically modeled as spatially uncorrelated but temporally correlated movements. An example of autonomous movements are settlement movements of benchmarks that are used in a leveling network, see for example Sect. 6.5.4. A well-known settlement model is the Koppejan model (Verruijt and van Baars, 2005), which models the settlement as a logarithmic function of time. Since $\lim_{t\to\infty} \log_{10}(t) = \infty$, settlement behavior as a model imperfection is unbounded and therefore the variogram and its corresponding covariance function do not exist. Autonomous movements can stochastically be modeled as a random-walk process (Odijk and Kenselaar, 2003) or by an empirical covariance function (Houtenbos, 2004):

$$\sigma^2_{s_i^t} = \sigma_s^2 |t - t_0|^{2p}, \qquad \sigma_{s_i^t s_i^u} = \frac{1}{2}\sigma_s^2 (|t - t_0|^{2p} - |t - u|^{2p} + |u - t_0|^{2p}), \tag{2.19}$$

where t_0 is the reference time before the start of the subsidence, t and u are points in time, and p is the power of the empirical covariance function. If $p = 0.5$, this empirical covariance function reduces to the random walk model, see e.g., Chatfield (1989). In the estimation of subsidence due to gas extraction from leveling measurements in Groningen for 2003, noise due to autonomous benchmark movements was set to 0.2 mm/$\sqrt{\text{yr}}$ (Schoustra, 2004).

Model imperfections due to uncertainties in the parameterization of the subsidence signal or its prognosis can be stochastically described by a covariance function as well. An example is the covariance function from Houtenbos (2004) that models spatially and temporally correlated deviations between measurements and the subsidence prognosis:

$$\sigma_{z_i^t z_i^u} = \frac{1}{2}\sigma_z^2 (|t - t_0|^{2p} - |t - u|^{2p} + |u - t_0|^{2p}) e^{-(l_{ij}/L)^2}, \tag{2.20}$$

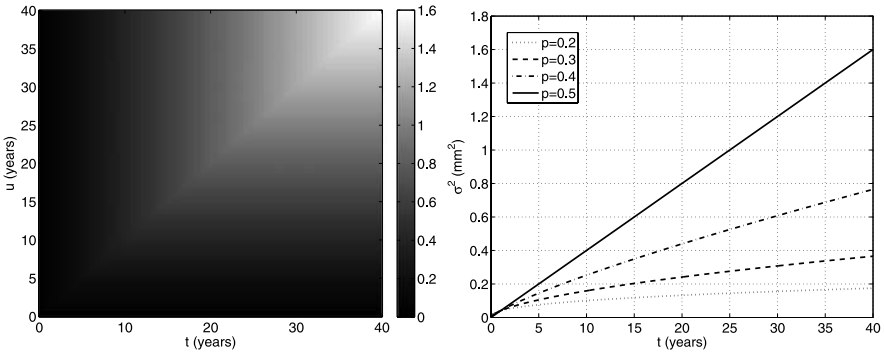

Fig. 2.8 Left: covariance induced by stochastically modeled autonomous movements ($p = 0.5$, $\sigma = 0.2$ mm) according to (2.19). The covariance due to autonomous movements increases in time. Right: variance of autonomous movements for different values of the power p. If p is equal to 0.5, the variance increases linear in time. If p is less than 0.5, the increase in variance reduces with increasing time (settlement behavior)

where $\underline{z}_i^t$ represents the model imperfection of point i at time t; $E\{\underline{z}_i^t\} = 0$. The distance between the points i and j is given by l_{ij}. In (2.20), model imperfections are modeled with a power model in time and an exponential covariance function in space. The exponential covariance function in space models the deviations that have a spatial correlation of length L. Due to the depth of the gas fields of ~3 km, a correlation length of at least 3 kilometers is expected for the deformation signal. The correlation length was set to 4 kilometers in the estimation of subsidence due to gas extraction in 2003 (Schoustra, 2004), to cover all spatially correlated deformation signal. The power model in time takes random walk deviations into account that are caused by an under- or overestimation of the subsidence prognosis in time.

The functional and stochastic modeling contributes to the precision and reliability of a measurement technique for monitoring the deformation signal of interest. Therefore, model imperfections will be further addressed in Sect. 6.5 as a part of the quality assessment.

2.3.4 Deformation Analysis of Subsidence Due to Gas Extraction

Both the point-wise multi-epoch (Sect. 2.3.2) and the continuous spatio-temporal deformation analysis (Sect. 2.3.3) have been applied in the Netherlands by gas and oil companies for monitoring subsidence due to hydrocarbon production.

Point-wise multi-epoch deformation analysis has the advantage that it provides direct insight in the movements of individual benchmarks. An example of point-wise multi-epoch deformation analysis in Groningen is the analysis of subsequent benchmark heights obtained from leveling campaigns (de Heus et al., 1994). A disadvantage of this method is that the benchmark heights are dependent on the choice of the reference benchmark(s). Furthermore, 2% of the benchmarks disappear yearly

which results in incomplete time series (Schoustra, 2004). Moreover, the spatio-temporal correlation of the deformation signal of interest is not utilized.

When modeling subsidence as a continuous spatio-temporal phenomenon (see Sect. 2.3.3), incomplete time series can easily be incorporated. Furthermore, due to the introduction of the spatio-temporal correlation of subsidence, outliers, identification errors and autonomous benchmark movements can be detected and removed in an automatic way. Finally, there is no dependency on the choice of the reference benchmark(s) due to the usage of the height difference measurements as the basic observations.

Methodologies that apply the continuous spatio-temporal deformation analysis concept are described by Kenselaar and Quadvlieg (2001) and Houtenbos (2004). The Subsidence Modeling (SuMo) concept of Kenselaar and Quadvlieg (2001) models the subsidence signal z as a (superposition of) ellipsoidal bowl(s) with decreasing linear benchmark velocities from the center of the bowl. The Subsidence Residual modeling (SuRe) concept of Houtenbos (2004) uses subsidence prognosis grids based on geomechanical modeling of the subsurface.

The mathematical framework underlying both SuMo and SuRe can be summarized as:

$$\underline{h}_{ij}^{t} = H_j^{t_0} - H_i^{t_0} + z_j^{t_0 t} - z_i^{t_0 t} + \underline{\delta h}_{ij}^{t} + \underline{\delta s}_j^{t} - \underline{\delta s}_i^{t} + \underline{\delta z}_j^{t_0 t} - \underline{\delta z}_j^{t_0 t}, \tag{2.21}$$

where $\underline{h}_{ij}^{t}$ is the spatial height difference observation between points i and j at time t, and $H_j^{t_0}$ and $H_i^{t_0}$ are the unknown initial heights. The functional model of subsidence due to gas extraction is denoted by z. When using prognosis grids, z is subtracted from the height difference observations, which results in subsidence residuals (SuRe). The stochastically modeled components are $\underline{\delta h}$ (measurement noise), $\underline{\delta s}$ (autonomous movements) and $\underline{\delta z}$ (subsidence model imperfections). In the SuRe methodology, the parameters of these stochastically modeled components are estimated through variance component estimation. Examples of stochastic parameters are variance factors, spatial correlation length and temporal power, see (2.20). An application of the SuRe concept including VCE is described in Sect. 6.5.4.2. Here, deformation components in Rotterdam are separated into autonomous movements and spatio-temporally correlated deformation signal.

Although continuous spatio-temporal deformation analysis has clear advantages, it is essential that the covariance function(s) that describe the model imperfections are adequate for the estimation of the signal of interest. If not, a risk exists of the attribution of displacement components to the wrong deformation cause. Hence, the link to geomechanics should be prominent in continuous spatio-temporal deformation analysis.

2.4 Conclusions

This chapter has summarized the geological and geomechanical properties of hydrocarbon reservoirs, and has focused specifically on the Groningen gas field in

the Netherlands. Based on the reservoir properties and production scenarios, the subsidence pattern at ground level can be predicted. The resulting subsidence is dependent on the geometrical shape of the reservoir, the compaction coefficient, the thickness of the reservoir, the pressure drop in the reservoir, and the geomechanical behavior of the overburden. Several methodologies are available to predict subsidence: from analytical expressions as a function of a few reservoir parameters to finite element analyses that take the spatially varying geomechanical parameters in the subsurface into account.

Geodetic techniques, such as leveling, are applied to measure deformation at ground level. Therefore, the subsidence signal is discretizised by a set of measurement points, that are monitored at subsequent epochs. Two types of deformation analysis have been addressed: point-wise multi-epoch and continuous spatio-temporal deformation analysis. Point-wise multi-epoch deformation analysis estimates deformation in time for each benchmark individually. Continuous spatio-temporal deformation analysis incorporates the spatio-temporal correlation of the signal of interest. When the functional model of the deformation signal is not well known, model imperfections can be modeled stochastically. To conclude, the applied deformation analysis methodologies in the Netherlands have been summarized.

Chapter 3 will focus on Persistent Scatterer InSAR as a measurement technique that can be applied for deformation monitoring from a geodetic point of view. The overview of deformation estimation concepts that have been presented in this chapter will be applied in the interpretation of InSAR displacement estimates in Sects. 4.5 and 6.5, and in the integration of InSAR and leveling deformation estimates in Chap. 7.

http://www.springer.com/978-1-4020-9427-9

Satellite Radar Interferometry
Subsidence Monitoring Techniques
Ketelaar, V.B.H.G.
2009, XVI, 244 p. 139 illus., 46 illus. in color., Hardcover
ISBN: 978-1-4020-9427-9